Post-Print

This is the accepted version of:

C.L. Bottasso, C.E.D. Riboldi
Estimation of Wind Misalignment and Vertical Shear from Blade Loads
Renewable Energy, Vol. 62, 2014, p. 293-302
doi:10.1016/j.renene.2013.07.021

The final publication is available at https://doi.org/10.1016/j.renene.2013.07.021

Access to the published version may require subscription.

When citing this work, cite the original published paper.

Estimation of wind misalignment and vertical shear from blade loads

C.L.Bottasso*, C.E.D.Riboldi

Dipartimento di Ingegneria Aerospaziale, Politecnico di Milano, Milano, Via La Masa 34, 20156 Italy

Abstract

This paper describes the formulation and verification of a novel observer of wind parameters. The general idea behind the proposed approach is to consider the wind turbine rotor as an anemometer. In fact, the rotor responds to varying wind conditions; by properly interpreting this response, one can indirectly measure some desired wind characteristics, as for example yaw and shear, as described here.

Measurements of wind conditions obtained this way are not affected by the usual disturbances of existing sensors, for example when installed in the nacelle or in the rotor wake. Furthermore, the approach provides rotor-equivalent quantities, and not the typical point information provided by wind vanes, anemometers or other similar sensors, whose information might be too local for large rotors.

The proposed method is here formulated for the observation of wind direction and vertical shear. The new observer is demonstrated first in a comprehensive simulation study using high-fidelity aeroservoelastic models, and then experimentally using an aeroelastically scaled wind tunnel model.

Keywords:

Wind observer, Wind misalignment, Wind shear, Wind turbine control, Aeroelasticity

Notation

a	Axial induction factor
c	Blade chord
C_{l_α}	Lift curve slope
e	Blade equivalent hinge offset
g	Gravitational acceleration
I_b	Equivalent flap inertia
K	Non-dimensional flapping frequency
K_1	Vertical wind shear gradient

*Corresponding author, *Tel.:* +39-02-2399-8315; *Fax:* +39-02-2399-8334.
Email address: carlo.bottasso@polimi.it (C.L.Bottasso)

K_β	Equivalent flap stiffness
l	Yaw moment arm, i.e. distance between yaw axis and rotor center
m	Blade bending moment
M_b	Blade mass
N	Number of revolutions for signal demodulation
$N_\mathcal{I}$	Number of observations in identification data set $\mathcal{I}$
$N_\mathcal{V}$	Number of observations in verification data set $\mathcal{V}$
q	Yaw rate
R	Rotor radius
t	Time
U_0	Cross-flow
V_0	Free-stream wind speed
x_g	non-dimensional span-wise center of gravity location
$\boldsymbol{M}$	Matrix of measured driving inputs
$\boldsymbol{T}$	Matrix of unknown model coefficients
$\boldsymbol{W}$	Matrix of measured wind parameters
$\mathcal{I}$	Identification data set
$\mathcal{V}$	Verification data set
β	Blade flap angle
β_0	Coning angle
γ	Lock number
λ	Non-dimensional inflow
Ω	Rotor angular speed
ψ	Azimuth angle
ρ	Air density
θ_p	Blade pitch
φ	Misalignment angle, $\varphi = \text{atan}(U_0, V_0)$
$(\cdot)^T$	Transpose
$(\cdot)^{\text{I}P}$	Rotor in-plane component
$(\cdot)^{\text{O}P}$	Rotor out-of-plane component
$(\cdot)_b$	Quantity pertaining to blade b
$(\cdot)_k$	Quantity pertaining to the kth trim point
$(\cdot)_{1c}$	First cosine harmonic
$(\cdot)_{1s}$	First sine harmonic

$\bar{(\cdot)}$	Non-dimensional quantity
$(\cdot)'$	Derivative wrt azimuthal angle, $\mathrm{d}\cdot/\mathrm{d}\psi$
$(\cdot)''$	Second derivative wrt azimuthal angle, $\mathrm{d}^2\cdot/\mathrm{d}\psi^2$
BEM	Blade element momentum
FBG	Fiber Bragg grating
HAWT	Horizontal axis wind turbine
LiDAR	Light detection and ranging
LQR	Linear quadratic regulator
MBC	Multi-blade coordinate
MW	Mega Watt

1. Introduction and motivation

In addition to wind speed, the knowledge of wind parameters such as direction and shears can be useful for control purposes. In fact, wind direction information drives yaw control that reduces the misalignment between wind and rotor. On board wind turbines, yaw control is needed because operation at high yaw angles causes a number of undesirable effects. For instance, the power available in the wind incident over the rotor is reduced with the third power of the cosine of the yaw angle; to give an example, operating at 20 deg of yaw reduces the available power of about 17%. Furthermore, yawed flow changes the angle of attack of the airfoils, which can further degrade aerodynamic performance besides the cosine effect mentioned above. In addition, wind-rotor misalignment generates side-side loads that tend to excite low damped modes of the machine, thereby inducing loads and vibrations, which in turn increase fatigue damage to the machine components.

Although it would appear beneficial to operate at low yaw because of the above reasons, these effects need to be carefully weighed against the cost of frequent yaw actuation. In fact, yawing the nacelle and rotor of a modern large wind turbine requires moving a very massive structure (for example weighing in excess of 150 tons for a typical 3.0 MW machine), overcoming the static friction in the yaw bearing when initiating the maneuver and slowing down the motion once the new alignment is reached, while limiting gyroscopic and aerodynamic loads throughout the whole maneuver. Hence, to reduce cost, complexity, size and maintenance of the yaw actuation system, its duty-cycle must be carefully limited.

In practice, such trade-offs between operation in yawed flow and yaw actuation are translated into control policies that realign the machine only when the yaw error exceeds a sufficiently large predetermined threshold for a sufficiently long period of time. The fact that yawing is important for performance and loads, but must be done only when really necessary because of the reasons noted above, implies that one would like to have precise and reliable measurements of the yaw angle, so as to yaw only for the right reason, of the right amount and at the right time.

Unfortunately, high-quality measurements of yaw are difficult to obtain. In fact, onboard yaw sensors, typically wind vanes, are affected by various sources of inaccuracy, including disturbances caused by the rotor wake and its turbulence, the presence of the nacelle, the periodic passing of the blades upstream of the instrument, etc. Although most sensors can be calibrated for compensating these effects, it is well known that the resulting wind measures are typically not very reliable nor accurate. Furthermore, existing sensors, even when well compensated for all sources of error, can only provide *point* (i.e. extremely local) information, usually at hub height. For the very large diameters of modern wind turbines this limitation can provide for an additional source of error, and a more global view of the wind direction over the rotor disk would be more appropriate.

Although the use of wind shear information is not as straightforward nor commonly used as wind direction, it is reasonable to assume that good quality wind shear information could be profitably exploited. For example, wind shears could be used to enhance the performance of wind turbines by the scheduling of control gains, or to lower the loads induced by such non uniform inflow conditions, for example by providing a feed-forward input that might be used for individual blade pitch control. Additional applications are foreseeable in wind farm control by the gathering of shear information throughout a wind farm without the need for additional sensors, by simply using the wind turbines as anemometers.

Goal of the present work is the development and testing of a yaw and vertical shear observer that overcomes the limitations of currently available point-wise sensors. To our knowledge this problem has not yet been successfully solved before. The approach proposed herein uses the whole rotor, and more specifically the blade loads, to infer these wind states. This way all limitations of current sensors are removed, including the one regarding the localized information that they provide.

The idea of designing observers to support the operation of wind turbine control systems and overcoming the inherent limitations of anemometers has been explored in the past, although limitedly to the observation of the wind speed, as for example in Refs. [12, 13, 14]. The problem is typically solved by using the dynamic torque balance equation of the rotor; by measuring the rotor speed and blade pitch, one can infer from that single equation, typically using a Kalman filter, an estimate of the wind effective (i.e., averaged throughout the rotor response) speed.

Generalized wind observers that can estimate various wind states, including wind speed, vertical and horizontal shear and yaw, have been described in Refs. [4, 5, 15]. The generalized approach uses a larger number of dynamic equilibrium equations, by adding to the torque balance also the fore-aft, side-side and blade flap dynamic equilibrium. This expanded set of equations allows one to reconstruct, again with a Kalman filter, a richer picture of the spatial distribution of the wind over the rotor disk. However the formulation is complicated and occasionally not fully robust, due to the fact that multiple wind states have in general a low level of observability; in fact, using that approach, it is at times hard to discriminate from

one another the effects of the various wind states from the response of the machine.

Here we develop a different and simpler approach that exhibits improved accuracy and robustness with respect to the one of Refs. [4, 5, 15], and overcomes the low observability problem. The new method is based on the first order harmonic blade response. In fact, by using a simplified model of a flapping blade, it is shown here that blade harmonics have a specific dependence on the wind characteristics and that each wind state, for example shear or yaw, leave a specific recognizable mark on the harmonic response of the blades. By using this fact, one can reliably infer at all times those wind states, simply by looking at the first harmonics of blade loads. These quantities can be readily obtained by processing on-line measurements obtained by suitable sensors, such as strain gages or optical fibers.

The paper starts off by showing the observability of yaw and shear by inverting the 1P response of an analytical blade flapping model. This derivation provides the structure that an observation model of these wind parameters could have, but it is not applicable in practice for the intrinsic limitations and simplifications underlying the analytical model. To overcome this problem, a more general observation model is then proposed, that maintains the same structure of the analytically derived one, but whose parameters are obtained by system identification, here based on a least-squares approach.

At first, the main characteristic of the formulation are assessed in a simulation environment, using comprehensive high-fidelity aeroservoelastic models, by looking at the simultaneous observability of both yaw and shear, at the quality of the estimates, and their independence from other varying wind parameters such as speed and turbulence. Specific tests also illustrate the use of corrective terms in the formulation that account, during a realignment maneuver, for the effects on the blade response of gyroscopic loads caused by the yawing of the rotor. Finally, the yaw observation formulation is tested on an aeroelastically-scaled wind tunnel model. The scaled model provides the means for an experimental verification of the proposed methodology in the controlled environment of the wind tunnel, as an intermediate step towards testing in the field.

2. Definition of the observation model structure from an analytical blade response model

The equations of dynamic equilibrium for a flapping hinged rigid blade, as derived in [9], write

$$\beta'' + \frac{\gamma}{8}\left(1 - \frac{4}{3}\cos\psi(\bar{U}_0 + \bar{q}\bar{l})\right)\beta' + \left(K + 2B\cos\psi + \frac{\gamma}{6}\bar{U}_0\sin\psi\right)\beta = \frac{\gamma}{2}\left(A - \frac{\bar{q}}{4}\sin\psi\right) - 2\bar{q}\cos\psi - \frac{\gamma}{2}\left((\bar{U}_0 + \bar{q}\bar{l})\left(\frac{\lambda}{2} + \frac{2\theta_p}{3}\right) + \frac{K_1\bar{V}_0}{4}\right)\cos\psi, \quad (1)$$

where $(\cdot)' = \mathrm{d}\cdot/\mathrm{d}\psi$ indicates a derivative with respect to the blade azimuthal angle $\psi = \Omega t$, while Ω is the constant angular velocity, $K = 1 + \epsilon + (K_\beta/I_b\Omega^2)$ is the non-dimensional flapping frequency, $\epsilon = M_b e x_g R^2/I_b$ a non-dimensional hinge offset term, $A = \lambda/3 + \theta_p/4$ an aerodynamic term accounting for non-dimensional

inflow $\lambda = (1-a)V_0/(\Omega R)$ and blade pitch setting θ_p, $G = gM_b x_g R/I_b$ and $B = G/2\Omega^2$ gravity terms, $\gamma = \rho C_{l_\alpha} cR^4/I_b$ the Lock number, $\bar{V}_0 = V_0/(\Omega R)$ the non-dimensional free-stream, $\bar{U}_0 = U_0/(\Omega R)$ the non-dimensional cross-flow, K_1 the vertical wind shear gradient, while $\bar{q} = q/\Omega$ is the non-dimensional yaw rate and $\bar{l} = l/R$ the non-dimensional yaw moment arm (cf. [9] for details).

Assuming a Fourier series solution arrested to the first order, i.e.

$$\beta = \beta_0 + \beta_{1c}\cos\psi + \beta_{1s}\sin\psi, \tag{2}$$

substituting it into Eq. (1) and collecting terms to match the harmonic coefficients of the unknowns β_0, β_{1c} and β_{1s}, while dropping higher harmonic terms in the process, one gets the solving system

$$\begin{bmatrix} K & B & 0 \\ 2B & K-1 & \gamma/8 \\ \gamma\bar{U}_0/6 & -\gamma/8 & K-1 \end{bmatrix} \begin{Bmatrix} \beta_0 \\ \beta_{1c} \\ \beta_{1s} \end{Bmatrix} = \begin{Bmatrix} \gamma A/2 \\ -\gamma\left((\bar{U}_0 + \bar{q}\bar{l})A_3/2 + K_1\bar{V}_0/4\right) - 2\bar{q} \\ -\gamma\bar{q}/8 \end{Bmatrix}, \tag{3}$$

where $A_3 = \lambda/2 - 2\theta_p/3$.

Before moving further, it is worthwhile noticing that the coning β_0 is largely unaffected by cross-flow and shear, as well as gravity. In fact, as shown in [9], considering shear but no cross-flow nor gravity, by solving (3) one gets

$$\beta_0 = \frac{\gamma A}{2K}. \tag{4}$$

Notice that coning is independent from the shear gradient K_1. Considering now cross-flow but no shear, one has

$$\beta_0 = \frac{\gamma A}{2\Delta}\left((K-1)^2 + \left(\frac{\gamma}{8}\right)^2\right) + \frac{\gamma A_3}{2\Delta}\left(B\bar{U}_0(K-1)\right), \tag{5}$$

where the determinant of (3) in the present case is

$$\Delta = K\left((K-1)^2 + \left(\frac{\gamma}{8}\right)^2\right) - 2B^2(K-1) + \left(\frac{\gamma}{8}\right)^2 \frac{4}{3}\bar{U}_0 B. \tag{6}$$

Inserting typical values for the relevant coefficients, one can easily verify that the terms due to cross-flow $\bar{U}_0$ and gravity B are small with respect to the other ones, so that the solution is very close to the one of Eq. (4). This result is in accordance with intuition, as it is expected that coning in a conventional wind turbine will be dominated by the average wind push orthogonally to the rotor plane, and much less so by in-plane wind components or wind gradients. Therefore, coning β_0 can be assumed to be a constant depending only on the considered trim point at a given free stream wind value.

Consider now only the second and third equations in the solving system (3), and rearrange terms to isolate the cross-flow $\bar{U}_0$ and vertical wind shear $K_1\bar{V}_0$, to get

$$-\gamma \begin{bmatrix} A_3/2 & 1/8 \\ \beta_0/6 & 0 \end{bmatrix} \begin{Bmatrix} \bar{U}_0 \\ K_1\bar{V}_0 \end{Bmatrix} = \begin{Bmatrix} 2B\beta_0 \\ 0 \end{Bmatrix} + \begin{bmatrix} K-1 & \gamma/8 \\ -\gamma/8 & K-1 \end{bmatrix} \begin{Bmatrix} \beta_{1c} \\ \beta_{1s} \end{Bmatrix} + \begin{bmatrix} 2+\gamma A_3\bar{l}/2 \\ \gamma/8 \end{bmatrix} \bar{q}. \tag{7}$$

Since this system is always invertible, from (7) one can compute the cross-flow and vertical wind shear as

$$\begin{Bmatrix} \bar{U}_0 \\ K_1\bar{V}_0 \end{Bmatrix} = \begin{Bmatrix} 0 \\ -16B\beta_0/\gamma \end{Bmatrix} + \begin{bmatrix} 3/4 & -6(K-1)/\gamma \\ -8(K-1)\beta_0/\gamma - 3A_3 & -\beta_0 + 24A_3(K-1)/\gamma \end{bmatrix} \begin{Bmatrix} \beta_{1c}/\beta_0 \\ \beta_{1s}/\beta_0 \end{Bmatrix} + \begin{bmatrix} -3/(4\beta_0) \\ -16/\gamma + A_3(3/\beta_0 - 4\bar{l}) \end{bmatrix} \bar{q}. \quad (8)$$

This result suggests the following remarks:

- Equation (8) is a linear observation model derived from the simple blade flap response model (1). Although not accurate enough for practical use, it suggests the *structure* that a blade-response-based observer of cross-flow and shear could have.

- Cross-flow and vertical wind shear can be computed on the sole knowledge of the 1P blade response (and possibly yaw rate, see below). This is due to the fact that cross-flow and shear induce different effects on the blade response, that ensure the invertibility of the left hand side matrix of system (7) and hence the observability of these two wind characteristics.

- The observation model depends on coefficients. These in turn depend on the aerodynamic and structural characteristics of the wind turbine, as well as on the operating condition through K, which depends on the rotor speed, and β_0 and A_3, which depend on wind speed and pitch setting. Hence, in general it can be expected that the coefficients of observation models of such structure should be scheduled with respect to wind speed in order to cover the whole operating envelope of a given machine.

  From Eq. (8), the form of the observation models of cross-flow and vertical shear that leads to the least variability in the model coefficients is

$$\bar{U}_0 = \begin{bmatrix} \frac{3}{4} & -6\,\frac{K-1}{\gamma} \end{bmatrix} \begin{Bmatrix} \beta_{1c}/\beta_0 \\ \beta_{1s}/\beta_0 \end{Bmatrix} - \frac{3}{4\beta_0}\,\bar{q}, \quad (9a)$$

$$K_1\bar{V}_0 = -\frac{16B\beta_0}{\gamma} + \begin{bmatrix} -8\,\frac{K-1}{\gamma} - 3\,\frac{A_3}{\beta_0} & -1 + 24\,\frac{A_3(K-1)}{\gamma\beta_0} \end{bmatrix} \begin{Bmatrix} \beta_{1c} \\ \beta_{1s} \end{Bmatrix} \quad (9b)$$

$$+ \left(-\frac{16}{\gamma} + A_3 \left(\frac{3}{\beta_0} - 4\bar{l} \right) \right) \bar{q}. \quad (9c)$$

  These expressions suggest that, in order to minimize the dependence of the model coefficients on the operating condition, one should be using as driving inputs β_{1c}/β_0 and β_{1s}/β_0 when estimating the cross-flow $\bar{U}_0$, and β_{1c} and β_{1s} when estimating the vertical shear $K_1\bar{V}_0$.

- The observation model of cross-flow depends only on K (when neglecting yaw rate), and hence the dependence of its coefficients on the operating condition is probably milder than in the case of wind

shear, at least within the accuracy of the present model problem. The term appearing in the shear model $A_3/\beta_0 = (4K/\gamma)(3\lambda - 2\theta_p)/(4\lambda + 3\theta_p)$ is also almost constant in the partial load region, where θ_p is null or very small, while it will present a greater variability in the full power region. In that same model, the non-homogenous term $-16B\beta_0/\gamma$ is probably the one that is expected to exhibit the highest degree of variability.

- The observation model considers the effects of yaw rate during a possible realignment maneuver. This exogenous forcing term corrects for the gyroscopic effects induced by yaw rate on the blade response and that, in its absence, would pollute the estimates of cross-flow and shear.

- The observation model assumes a steady state periodic response, possibly including a steady state yawing maneuver. However, due to ever present fluctuations in the wind, the response of a wind turbine is seldom in a steady state. Nevertheless, the present observer is still believed to provide useful information for control purposes. For example, yawing to eliminate cross-flow is customarily performed by filtering the wind direction information to eliminate short-term fluctuations, and by maneuvering only when a significant enough misalignment has been reached and maintained for a sufficient length of time. It is clear that, for this purpose, the fact that the observer is unable to account for unsteadiness in the response is most probably irrelevant. Similarly, wind shear information might be used for the scheduling of controllers or for providing feed-forward information. Here again, it is expected that the main effect of such strategies should be in the capturing of wind shear variations on rather slow time scales taking place over several rotor revolutions (and very often much more slowly, as for example in the day-night shear cycles). In this sense, depending on the time scale variations that need to be resolved for a given specific application, it is possible that the inclusion of the yaw rate in the observation model can be safely neglected. More in general, it can be assumed that the steady state assumption at the base of the observation model is largely acceptable for the scope of the present work.

3. Estimation of cross-flow and vertical shear from blade loads

3.1. A general observation model

The previous section has shown, by using a simplified analytical model, the possible structure of a linear parameter varying (wind-scheduled) observation model for cross-flow and vertical wind shear. To overcome the intrinsic limitations of the simplified analytical model, we propose here a general observation model that has a similar structure, but whose coefficients are identified from measurements of the wind characteristics and their associated blade response. The process by which such coefficients can be identified is described in §3.2.

Inspired by Eq. (8), a general wind-scheduled observation model of cross-flow and wind shear can be formulated as

$$\bar{\boldsymbol{w}} = \bar{\boldsymbol{w}}_0(V_0) + \boldsymbol{A}(V_0)\bar{\boldsymbol{m}} + \boldsymbol{B}(V_0)\bar{q}, \tag{10}$$

where $\bar{\boldsymbol{w}} = (\bar{U}_0, K_1\bar{V}_0)^T$ is the vector of observed wind quantities. Notice that, at this stage, the wind shear is not necessarily restricted to be the constant gradient of the analytical model, and in fact the power law will be used in all examples shown later on. $\bar{\boldsymbol{w}}_0(V_0) = (0, \bar{w}_2(V_0))^T$, $\boldsymbol{A}(V_0)$ and $\boldsymbol{B}(V_0)$ are the unknown to-be-identified coefficients of the linear observation model, that replace those provided by the simplified analytical model expressed in Eq. (8). As previously noted, all coefficients are expected to exhibit some degree of variability with respect to the free-stream wind V_0, and therefore are scheduled accordingly. Finally, the driving inputs are given by vector $\bar{\boldsymbol{m}}$ of 1P load harmonic amplitudes, which is defined as

$$\bar{\boldsymbol{m}} = (m_{1c}^{\mathrm{OP}}, m_{1s}^{\mathrm{OP}}, m_{1c}^{\mathrm{IP}}, m_{1s}^{\mathrm{IP}})^T, \tag{11}$$

as well as the yaw rate $\bar{q}$ during a maneuver.

The definition of driving inputs deserves some explanations:

- In Eq. (10), the blade root bending moments given in (11) are preferred to the blade flap amplitudes appearing in Eq. (8) because they provide an equivalent informational content while being more readily measurable on board wind turbines, as for example by means of strain gages or Fiber Bragg Grating (FBG) sensors.

- Both out-of-the-rotor plane (superscript $(\cdot)^{\mathrm{OP}}$) as well as in-plane (superscript $(\cdot)^{\mathrm{IP}}$) blade root components are used in (11), in contrast with the sole out-of-plane blade flap angle of model problem (8). In fact, the model problem formulation assumes that the blade flaps orthogonally to the rotor plane [9]; while this assumption is reasonable at low wind speeds in the partial load region, it becomes progressively more inaccurate as the blade is pitched in the transition and full load regions. The addition of the in-plane blade response greatly improves the observability of the wind characteristics at higher wind speeds, as verified in practice in the experiments described later on in this work.

- Finally, following the suggestion of expressions (9), the driving bending moment 1P harmonics (11) are scaled by the zeroth harmonic for the observation of cross-flow, while they are not scaled in the case of the vertical wind shear.

3.2. Observer synthesis by identification

The generic observation model expressed by Eq. (10) is defined in terms of unknown wind-dependent coefficients that should be identified by means of suitable observations of the wind characteristics and their associated blade response. Such measurements can in principle be obtained in two ways:

1. Using the target wind turbine. This *model-free* approach requires the measurement in the field of wind speed, cross-flow and wind shear (for example, by met towers, LiDAR or other devices) and the synchronous measurement of blade root loads (for example, by strain gages, optical fibers, or other devices).
2. Using a sufficiently accurate aeroelastic model. This *model-based* approach requires the conduction of a number of numerical simulations, whereby the aeroelastic model is subjected to wind fields of known characteristics in terms of speed, cross-flow and vertical shear, while recording the associated computed blade loads.

Both approaches have possible advantages and disadvantages, and both are demonstrated later on in the present paper. For the first, high quality field measurements of all necessary quantities might not always be readily available. This problem is circumvented in the second approach, since it is easy to conduct all necessary virtual experiments in a simulation environment so as to gather all required data for the synthesis of the observation model. On the other hand, for the second approach one should keep in mind that model errors, i.e. possible mismatches between the aeroelastic model and the real wind turbine, might affect the quality of the estimates. Therefore, one should verify that the aeroelastic model used in the virtual experiments is capable of capturing the effects that cross-flow and wind shear have on the 1P blade response with sufficient accuracy.

The identification of the unknown model coefficients can be obtained by a standard least-squares procedure. To this end, Eq. (8) can be written collectively for all available observations and associated driving inputs in the identification set $\mathcal{I} = \{\bar{\boldsymbol{w}}_i, \bar{\boldsymbol{m}}_i, \bar{q}_i, i = 1, \ldots, N_{\mathcal{I}}\}$, as

$$\boldsymbol{W} = \boldsymbol{T}(V_0)\boldsymbol{M}, \tag{12}$$

where the input and output matrices are defined as

$$\boldsymbol{W} = \left[\bar{\boldsymbol{w}}_1, \bar{\boldsymbol{w}}_2, \ldots, \bar{\boldsymbol{w}}_{N_{\mathcal{I}}}\right], \tag{13a}$$

$$\boldsymbol{M} = \left[\begin{Bmatrix} 1 \\ \bar{\boldsymbol{m}}_1 \\ \bar{q}_1 \end{Bmatrix}, \begin{Bmatrix} 1 \\ \bar{\boldsymbol{m}}_2 \\ \bar{q}_2 \end{Bmatrix}, \ldots \begin{Bmatrix} 1 \\ \bar{\boldsymbol{m}}_{N_{\mathcal{I}}} \\ \bar{q}_{N_{\mathcal{I}}} \end{Bmatrix}\right], \tag{13b}$$

while, for each given wind speed V_0, the matrix of unknown coefficients is defined as

$$\boldsymbol{T}(V_0) = \left[\bar{\boldsymbol{w}}_0(V_0), \boldsymbol{A}(V_0), \boldsymbol{B}(V_0)\right]. \tag{14}$$

Having a sufficient number of independent observations in set $\mathcal{I}$ in order to cover a desired range of cross-flow and shear values, possibly considering a sufficient number of different yaw rate conditions, Eq. (12) can be solved by least-squares to yield the desired estimates of the model coefficients at a given wind speed as

$$\boldsymbol{T}(V_0) = \boldsymbol{W}\boldsymbol{M}^T(\boldsymbol{M}\boldsymbol{M}^T)^{-1}. \tag{15}$$

Having an independent set $\mathcal{V} = \{\bar{\boldsymbol{w}}_j, \bar{\boldsymbol{m}}_j, \bar{q}_j, j = 1, \ldots, N_{\mathcal{V}}\}$ of additional observations and associated driving inputs, $\mathcal{V} \cap \mathcal{I} = \emptyset$, one can readily verify the quality and generality of the identified model by computing the modeling errors

$$\boldsymbol{e}_j = \bar{\boldsymbol{w}}_j - \boldsymbol{T}(V_0)\bar{\boldsymbol{m}}_j, \quad j = 1, \ldots, N_{\mathcal{V}}. \tag{16}$$

3.3. Observer implementation

Once all model coefficients have been identified, for example as explained above, the wind observer can be used to estimate cross-flow and/or wind shear, as necessary. To this end, one must first compute the driving 1P load harmonics appearing in the input vector $\bar{\boldsymbol{m}}$. This can be done in at least two alternative ways.

The first is to demodulate by projection the blade root bending moment components, as obtained by the on-board sensors, independently on the three blades. For the bth blade, this process can be carried out at each time step by using data collected over the previous N rotor revolutions:

$$m_{0_b} = \frac{1}{2N\pi} \int_{\psi}^{\psi - 2N\pi} m_b(t) \mathrm{d}\psi, \tag{17a}$$

$$m_{1c_b} = \frac{1}{N\pi} \int_{\psi}^{\psi - 2N\pi} m_b(t) \cos(\psi) \mathrm{d}\psi, \tag{17b}$$

$$m_{1s_b} = \frac{1}{N\pi} \int_{\psi}^{\psi - 2N\pi} m_b(t) \sin(\psi) \mathrm{d}\psi. \tag{17c}$$

Subsequently, an average of the resulting amplitudes is calculated over the three blades, i.e. $m_0 = 1/3 \sum_{b=1}^{3} m_{0_b}$ and similarly for the cosine and sine components. This approach provides for an effective filtering of rapid fluctuations and transients (effects enhanced by increased observation windows defined by N, clearly at the cost of increasing delays), and it was used for all examples discussed later on in Sect. 4.

A second possible approach is to compute the necessary amplitudes by using the multi-blade coordinate (MBC) transformation of Coleman and Feingold [8]. By this approach, the necessary amplitudes are readily computed as

$$\begin{Bmatrix} m_0 \\ m_{1c} \\ m_{1s} \end{Bmatrix} = \frac{1}{3} \begin{bmatrix} 1 & 1 & 1 \\ 2\cos\psi_1 & 2\cos\psi_2 & 2\cos\psi_3 \\ 2\sin\psi_1 & 2\sin\psi_2 & 2\sin\psi_3 \end{bmatrix} \begin{Bmatrix} m_1 \\ m_2 \\ m_3 \end{Bmatrix}, \tag{18}$$

where the azimuthal angle of the bth blade is $\psi_b = \psi_1 + 2\pi(b-1)/3$, for $b = 1, 2, 3$. The harmonic analysis of the effects of the above transformation shows that the Coleman-transformed components should be filtered around and above 3P to remove higher harmonics. This second approach will be investigated in a continuation of the present research.

Wind scheduling can be implemented as follows. An estimate of the instantaneous turbulent hub-height free-stream wind can be provided by a hub wind observer [12, 13, 14]; the estimated wind is then filtered, for example with a moving average, to remove fast fluctuations. Given the resulting current instantaneous wind

estimate V_0, the coefficients of the observation model are obtained by linear interpolation of the matrices that were identified at the trim points k and $k+1$, i.e.

$$\boldsymbol{T}(V_0) = (1-\xi)\boldsymbol{T}(V_{0_k}) + \xi\boldsymbol{T}(V_{0_{k+1}}), \tag{19}$$

with $\xi = (V_0 - V_{0_k})/(V_{0_{k+1}} - V_{0_k})$ and $V_0 \in [V_{0_k}, V_{0_{k+1}}]$.

4. Results

In the following, the proposed observer is tested at first in a simulation environment. The simulation approach has the purpose of illustrating the main characteristics of the proposed formulation with complete knowledge of the solution, and of the model-based approach to system identification. Next, the observer is tested with an aeroelastically-scaled wind turbine model [6] operated in the boundary layer wind tunnel of the Politecnico di Milano. This second set of results illustrates the use of actual measurement data, although not gathered in the field but in the controlled environment of the wind tunnel, as well as the model-free approach to system identification.

4.1. Results in a simulation environment

4.1.1. Model identification

We consider a 3MW HAWT, regulated by a collective-pitch/torque controller based on a speed-scheduled linear quadratic regulator (LQR) with integral state [15], and modeled in `Cp-Lambda`, a finite element multi-body wind turbine simulator [2, 3]. The model includes flexible blades, tower and drive-train/nacelle system, compliant foundations, and a classical BEM aerodynamic model enhanced with tip, hub and unsteady corrections, dynamic stall and tower-interference models.

The observation model was identified as previously explained. The identification data set included, for each wind speed between 3 and 25 m/sec in steps of 2 m/sec, operating conditions with different misalignment angles, ranging from -48 deg to +48 deg in rather large steps of 8 deg, with a shear power law exponent equal to 0.2. In addition, for a 0 deg misalignment, the data set included operating conditions characterized by shear exponents ranging from 0.0 to 0.4 in steps of 0.1. It was verified that, due to the independence of yaw from shear and viceversa, the addition to the identification data set of operating conditions at various wind shear and non-null yaw, did not improve the quality of the model and of the resulting estimates.

At first, a model was identified using only out-of-plane blade root loads, i.e. by using in Eq. (10) the input vector $\bar{\boldsymbol{m}} = (m_{1c}^{\mathrm{OP}}, m_{1s}^{\mathrm{OP}})^T$. The results presented in Fig. 1 show a comparison, for increasing free-stream wind speeds V_0, between the actual values of $\bar{U}_0$ used in each simulation (horizontal axis) and the estimated ones $\bar{U}_0^*$ (vertical axis). A perfect identification would result in the linear solid line shown in the graph. The plot shows good fidelity of the estimates at low wind speeds, and a progressive severe degradation at the

higher ones. As previously explained, it appears that, as the blade is pitched into the wind, the sole use of the out-of-plane loads is not capable of correctly observing the wind cross-flow.

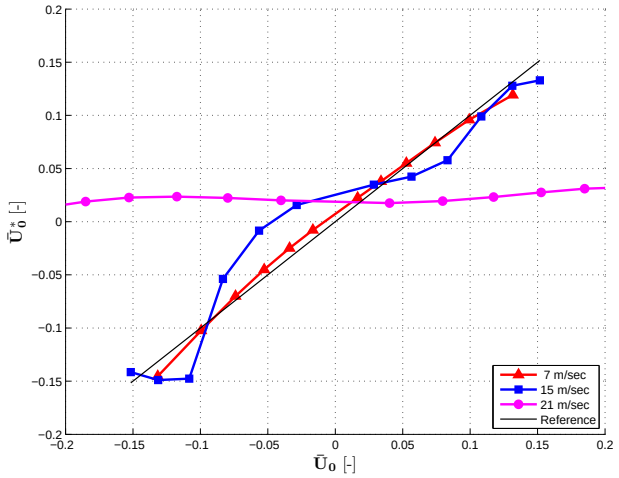

Figure 1: Verification of cross-flow observability using only out-of-plane bending moments.

The effect noted above is corrected by including in the observation model inputs also the in-plane load components. After having identified a new model, the previous verification was repeated, yielding the results shown in Fig. 2. In this case, good observability of wind cross-flow is obtained throughout the entire operating envelope of the machine; some non-linearity appears to be present at the higher wind speeds.

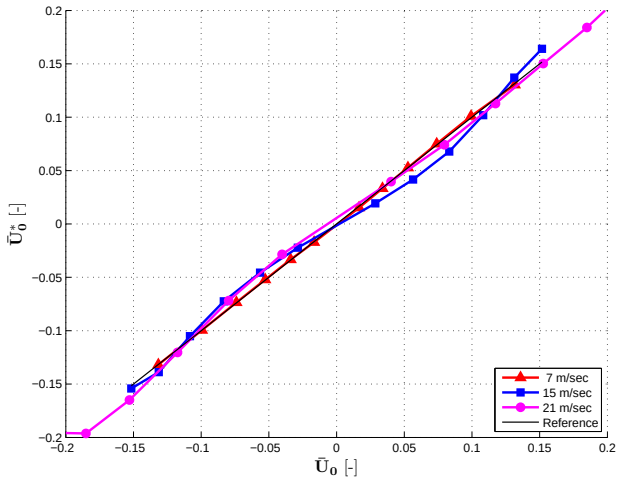

Figure 2: Verification of cross-flow observability using out-of-plane and in-plane bending moments.

4.1.2. Observation results

To test the quality of the reconstruction, a set of increasingly demanding simulations was carried out.

At first, we consider the effect of varying wind direction, together with a simultaneous varying wind shear. These tests have the purpose of showing that indeed, as predicted by the model problem, variations in shear do not affect cross-flow estimates and viceversa. For clarity, these first tests are conducted in non-turbulent wind conditions. The hypothesized independence between cross-flow and shear is confirmed by Fig. 3, which reports the results of a simulation at 15 m/sec of mean hub wind, where the power law wind shear was changed between 0.1 and 0.4. [CEDR] The wind direction estimate is always precise and exhibits a little delay of about 4.8 sec, even in the presence of fast shear variations. This delay compares well with the time necessary for a revolution of the rotor, and is much lower than the characteristic time normally adopted for yaw control. Similarly, the shear estimate is also precise, even in the presence of fast wind direction changes.

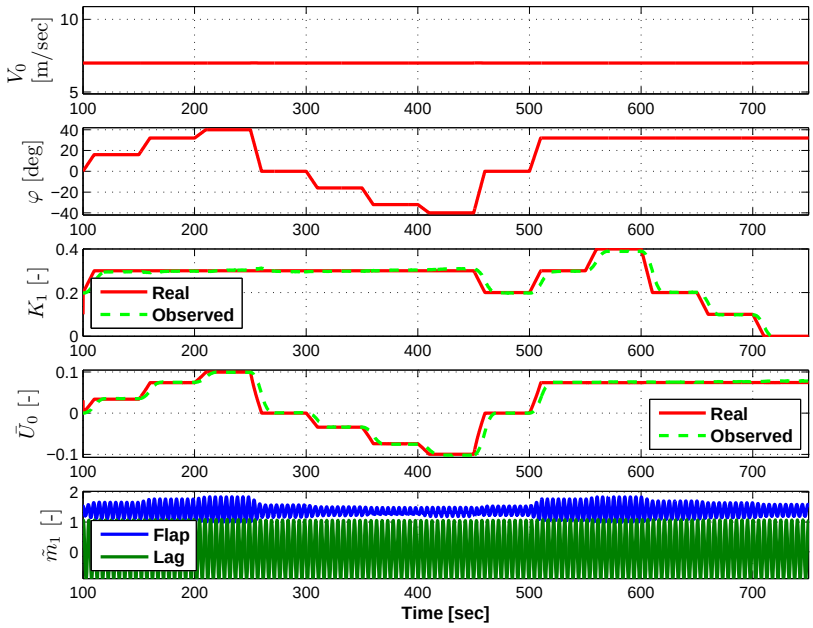

Figure 3: Observation in non-turbulent conditions, for varying wind shear.

To understand the effects of wind scheduling on the performance of the observer, the same yaw and shear time histories of the previous trial were used together with a changing free-stream speed. Figure 4 reports the various time histories as well as the results. To make things harder, the time histories were designed to exhibit synchronous sharp variations in yaw and wind speed at around 250 sec, as well as synchronous sharp variations in yaw, shear and wind speed at around 450 sec. These simultaneous changes in multiple wind parameters clearly induce a noticeable unsteadiness in the response of the wind turbine, which can be appreciated in the blade load responses shown in the bottom part of the figure. Since the observation model assumes a steady periodic condition, estimates are somewhat negatively affected by the unsteady response of the system soon after these events. Nonetheless, the overall behavior of the observer is still rather satisfying.

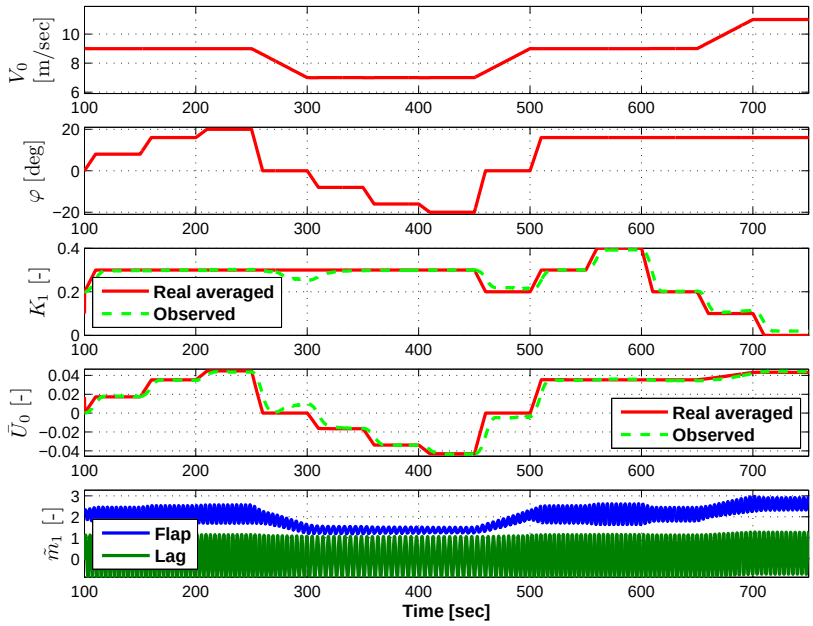

Figure 4: Observation in non-turbulent conditions, for varying wind shear and speed.

Next, the observer was tested in turbulent wind conditions.

A first trial was performed with a deterministic constant hub wind speed superimposed to a 15% intensity random disturbance, which is spatially-varying over the rotor disk. Time histories and results are reported in Fig. 5.

The estimated mean hub wind used for model interpolation was filtered with a moving average over a 5 sec window. To account for the random disturbances produced by turbulence, the blade root measurements were denoised with a zero-phase fourth-order Butterworth low-pass filter with a time constant of 1 sec. Furthermore, signal demodulation was performed over two rotor revolutions ($N = 2$ in Eq. (17)), which provides for an additional filtering effect.

The computation of the "real" value of cross-flow $\bar{U}_0$, reported in Fig. 5 as a solid line, deserves some explanation. In fact, even for a constant yaw (measured with respect to the deterministic wind component of the turbulent wind field), $\bar{U}_0 = U_0/(\Omega R)$ varies because of two effects: first Ω is not constant because of turbulence and of the response of the closed-loop controller, and secondly U_0 exhibits a spatial variation over the rotor disk. To account for these effects, here and in the following the "real" reference value of cross-flow $\bar{U}_0$ is computed at each time instant using the current rotor speed and by averaging U_0 over the lengths spanned by the three blades in their current azimuthal position.

The previous example was repeated with varying mean hub wind and more abrupt wind direction step changes. As shown in Fig. 6, here again the quality of the observation seems to be rather good, notwith-

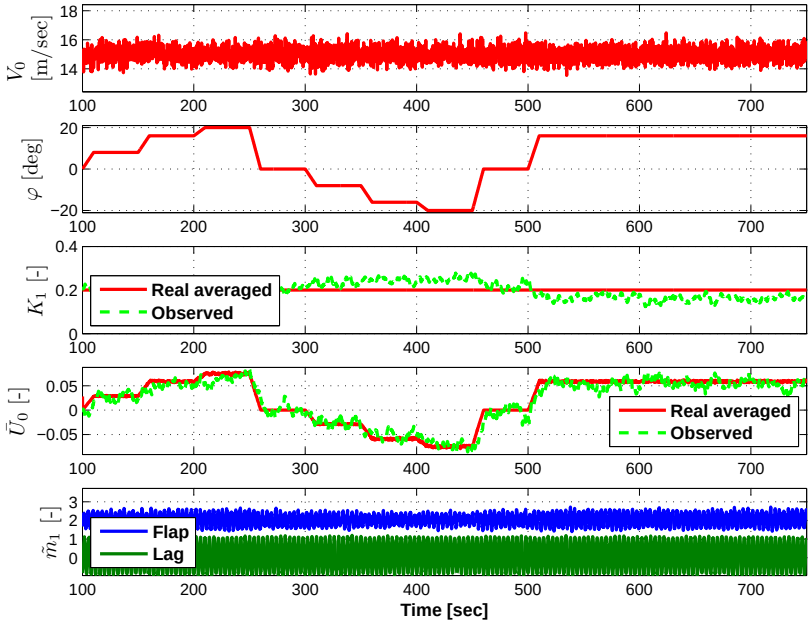

Figure 5: Observation in turbulent conditions, for constant wind shear and speed.

standing the effects of all disturbances and variations.

[CEDR] In these turbulent scenarios, the observation delay can be estimated at 8.3 and 11.0 sec respectively, more intense than in deterministic conditions due to the higher number of revolutions N considered for demodulation and to the moving average applied to the wind speed signal prior to interpolation. These delay is still not very relevant if compared to the characteristic time of yaw actuation.

Finally, the observer was tested with the turbulent wind fields described in Refs. [1, 10], using a turbulence intensity of 10% and the Kaimal model. Several simulations were performed with mean hub speeds ranging from 7 m/sec to 23 m/sec in steps of 4 m/sec, with mean yaw angles spanning from -32 deg to +32 deg in steps of 8 deg.

The use of more realistic turbulent wind conditions than those of the previous examples goes in the direction of providing simulation tests that are closer to reality, but raises some difficulties in the interpretation of the results. In fact, even if the mean wind field has a constant direction, eddies in the turbulent flow cause yaw variations at various spatial and temporal scales. Given the broad band of such eddies, it is difficult in this case to define a "true" yaw to be used for comparison with the rotor-effective estimates generated by the observer. To ease this problem, which deserves further investigation, only long-term estimates that somewhat filter the effects of such fluctuations are presented here. To this end, demodulation was performed over five rotor revolutions ($N = 5$), and the observed yaw was further filtered with a 50 sec moving average.

The results of the various observations are synthetically presented in Fig. 7 for simulations with mean

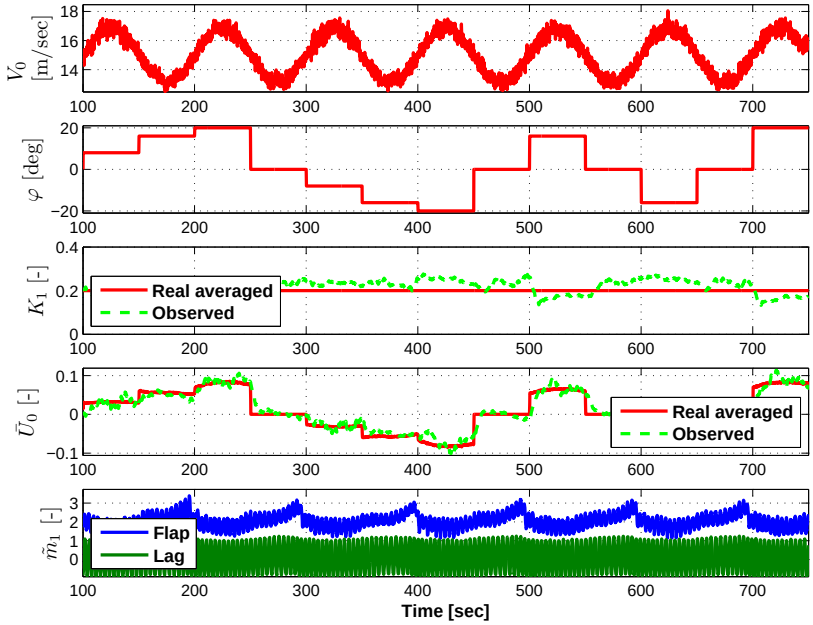

Figure 6: Observation in turbulent conditions, for varying mean hub wind speed.

wind speeds of 7, 11 and 15 m/sec. Every point on these plots corresponds to a 600 sec simulation in turbulent wind, with a given mean misalignment. Notice that, unlike previous plots, the yaw misalignment angle $\varphi = \text{atan}(U_0, V_0)$ is used here instead of the non-dimensional cross-flow $\bar{U}_0$. Results are reasonably good, with some more noticeable discrepancies at the larger yaw angles, but as previously mentioned a more rigorous analysis and a more precise definition of the ground truth might reveal a slightly different (possibly better) picture; this aspect will be further investigated in a continuation of the present research.

4.2. Effect of yaw rate driving input

The verification of the effects of a yaw rate driving input to correct for the gyroscopic effects during a realignment maneuver was carried out using a `FAST` [11] model of the NREL CART-3 wind turbine, using a PI collective-pitch/torque controller. The identification process was performed at average hub wind speeds between 5 and 25 m/sec in steps of 5 m/sec, with yaw angles between -48 and +48 deg in steps of 5 deg, and for yaw rates equal to 0, -0.35 deg/sec and +0.35 deg/sec.

Yaw observation was conducted in the following conditions. Initially, with the nacelle standing still, the wind stream was progressively yawed at a constant rate. After the wind had been yawed to 20 deg, the nacelle-rotor system started a realignment maneuver at a constant yaw rate. During this maneuver, the misalignment between rotor axis and wind was kept constant, by changing the absolute wind direction accordingly. After completion of the maneuver, the same was executed again in the opposite direction.

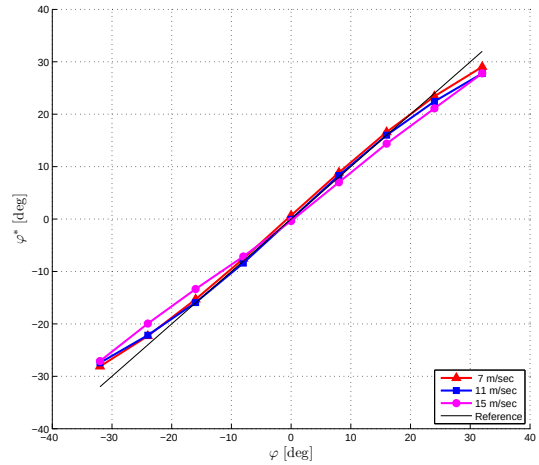

Figure 7: Observed yaw misalignments in turbulent Kaimal wind fields of 10% intensity.

Figure 8 shows the results obtained with and without the yaw rate driving input. As expected, in the latter case the observation of misalignment during the yawing maneuver is slightly less accurate, because of the presence of gyroscopic loads that affect the response of the blades.

4.3. Results using a scaled wind tunnel model

The proposed procedure was then tested on an aeroelastically-scaled wind tunnel model of the Vestas V90 wind turbine [6]. With respect to the full scale machine, the 1/45 scaled model matches its placement of the lowest three blade and two tower natural frequencies, its tip-speed ratio and Lock number. The rotor uses low-Reynolds airfoils and transition strips, reaching a maximum power coefficient of about 0.37, after correction to account for wind tunnel blockage. The model features individual blade pitch and torque control, and it is instrumented with blade root strain gages which provide measurements of blade bending moments, shaft strain gages for bending and torque, a six component balance at the tower base, rotor azimuth and blade pitch encoders, as well as a bi-axial nacelle accelerometer. Blade strain signals are acquired at 250 Hz, while the 1P frequency at rated speed is 6.08 Hz.

4.3.1. Model identification

Runs were conducted at different values of yaw between -30 deg and +30 deg in steps of 10 deg; these different yaw conditions were realized by bolting the model to the wind tunnel floor in the required different directions, as the model at present does not have direct yaw control. All runs were performed at the same tip speed ratio corresponding to a full power condition, with a constant rotor speed of 365 rpm, a mean hub wind speed of 8.5 m/sec, and a fixed pitch value of 5.35 deg. For the particular setup used in these tests, the

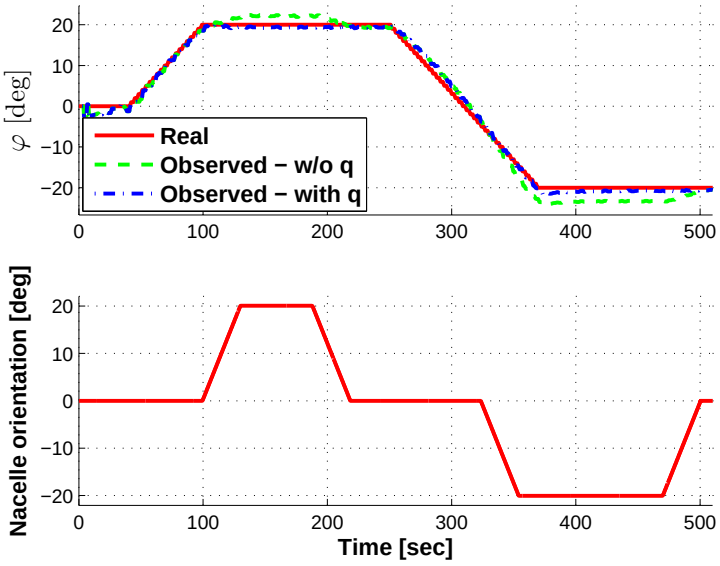

Figure 8: Misalignment observation during a yawing maneuver, with and without yaw rate driving inputs.

wind shear was almost null and the turbulence intensity around 1–2%. To remove the effects of turbulence and noise in the measurements, demodulation was performed over a rather long time window, using $N = 40$. The observation model is driven by both out-of-plane and in-plane blade loads.

The results of the identification performed on the scaled model are reported in Fig. 9, which shows an excellent correlation between real and estimated cross-flow parameters.

4.3.2. Observation results

A different set of similar runs was used for the verification of the observation capabilities. The observed yaw angles, averaged over a 30 sec time window, are reported in Fig. 10, showing here again an excellent quality of the estimates.

5. Conclusions

In this work we have proposed a new formulation for the observation of wind misalignment and vertical wind shear. The method uses the whole rotor as an anemometer, and tries to estimate the desired wind characteristics from its response, thereby providing rotor-equivalent effective estimates.

The analysis of a flapping blade model problem shows that yaw and shear can be simultaneously estimated from the blade load lowest harmonics. This result was used to formulate a more general wind-scheduled observation model, whose defining coefficients were identified by a least-squares technique.

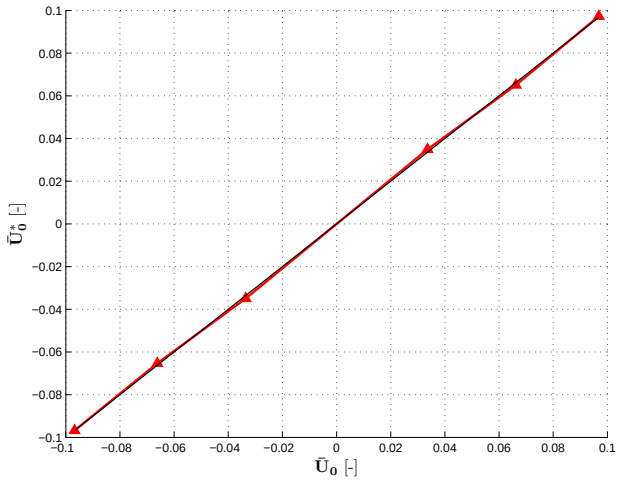

Figure 9: [CEDR] Correlation between real and observed non-dimensional cross-flow for the identification data set.

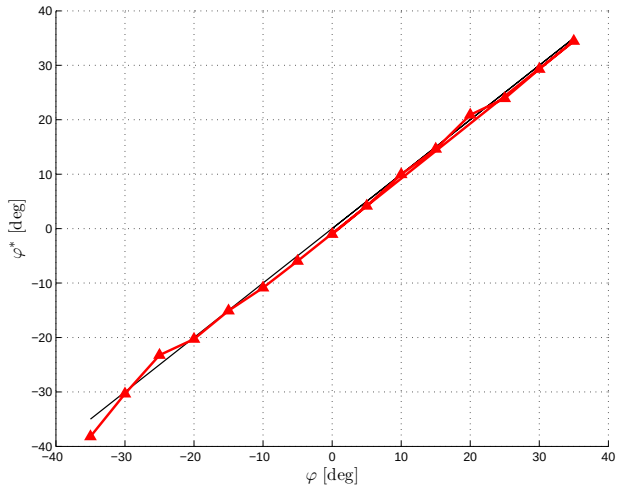

Figure 10: [CEDR] Correlation between real and observed misalignment angle for the verification data set.

From the results of the numerical and experimental verifications of the proposed procedure carried out so far, the following conclusions can be derived:

- Cross-flow and vertical shear are identifiable from the 1P blade harmonic response, even in the presence of simultaneous variations of these two quantities, of wind speed and turbulence.
- The observation is still of good quality in the presence of spatially and temporally varying stochastic disturbances of the wind field. For more realistic turbulent wind fields, judgement of the quality of the observations requires further investigations because of the lack of a clear definition of a ground truth.
- Correction of the effects of gyroscopic loading during a yaw maneuver can be achieved, although its real importance in applications might not be crucial.
- In general, it appears that good quality results can be obtained with the identification of the observation model from experiments performed by simulation on an aeroelastic model. While this eases the identification, since different data sets of known wind conditions and corresponding measurements can be easily generated, possible mismatches between the aeroelastic model and the actual plant might pollute the wind estimates and therefore affect the observation results. In this sense, the results of the model-based approach to identification of the observation model can only be as good as the aeroelastic model.
- The model-free approach to identification worked quite well for the wind tunnel experimental data sets. It remains to be seen how this approach performs using actual field data, where higher levels of turbulence might be expected than in the wind tunnel data used here.

Acknowledgements

This work is supported by the Alliance for Sustainable Energy LLC, National Renewable Energy Laboratory (NREL), sub-contract No. AGV-2-22481-01, technical monitor Dr. Alan D. Wright.

References

[1] Anonymous, Wind Turbines - Part 1: Design Requirements, International Standard IEC 61400-1, 2005.

[2] O.A. Bauchau, C.L. Bottasso, L. Trainelli, Robust integration schemes for flexible multibody systems, Computer Methods Appl. Mech. Eng. 192(2003) 395–420.

[3] C.L. Bottasso, A. Croce, Cp-Lambda: user's manual, Technical Report, Dipartimento di Ingegneria Aerospaziale, Politecnico di Milano, 2006–2012.

[4] C.L. Bottasso, A. Croce, Advanced control laws for variable-speed wind turbines and supporting enabling technologies, Technical Report DIA-SR 09-01, Dipartimento di Ingegneria Aerospaziale, Politecnico di Milano, 2009.

[5] C.L. Bottasso, A. Croce, C.E.D. Riboldi, Spatial estimation of wind states from the aeroelastic response of a wind turbine, in: The Science of Making Torque from Wind (TORQUE 2010), Forth, Heraklion, Crete, Greece, 2010.

[6] C.L. Bottasso, F. Campagnolo, A. Croce, L. Maffenini, Development of a wind tunnel model for supporting research on aero-servo-elasticity and control of wind turbines, in: 13th International Conference on Wind Engineering (ICWE13), Amsterdam, The Netherlands, 2011.

[7] C.L. Bottasso, A. Croce, Y. Nam, C.E.D. Riboldi, Power curve tracking in the presence of a tip speed constraint, Renew. Energy 40(2012) 1–12.

[8] R.P. Coleman, A.M. Feingold, Theory of self-excited mechanical oscillations of helicopter rotors with hinged blades, Technical Report, NACA TN 1351, 1958.

[9] D.M. Eggleston, F.S. Stoddard, Wind Turbine Engineering Design, Van Nostrand Reinhold Company Inc., New York, 1987.

[10] B. Jonkman, M. Buhl, TurbSim's user guide, Technical Report, National Renewable Energy Laboratory (NREL), Golden, CO, 2007.

[11] B. Jonkman, M. Buhl, FAST user's guide, Technical Report, National Renewable Energy Laboratory (NREL), Golden, CO, 2005.

[12] X. Ma, N.K. Poulsen, H. Bindner, Estimation of wind speed in connection to a wind turbine, Technical Report, Technical University of Denmark, 1995.

[13] X. Ma, Adaptive extremum control and wind turbine control, Ph.D. Thesis, Technical University of Denmark, 1997.

[14] K.Z. Østergaard, P. Brath, J. Stoustrup, Estimation of effective wind speed, J. Phys. (2007): Conference series: The Science of Making Torque from Wind; 75(012082).

[15] C.E.D. Riboldi, Advanced control laws for variable-speed wind turbines and supporting enabling technologies, Ph.D. Thesis, Politecnico di Milano, 2012.